Module 5

Charge exchange and beam emission spectroscopy. Modelling emitter populations, beam stopping and analysing spectra.

Lecture viewgraphs

Hugh Summers, Martin O'Mullane and Alessandra Giunta

University of Strathclyde

Contents

1.1 The edge-divertor plasma environment

The expanded schematic on the left shows the migration of deuterium into the plasma, starting from the release of molecular deuterium from the target zone.

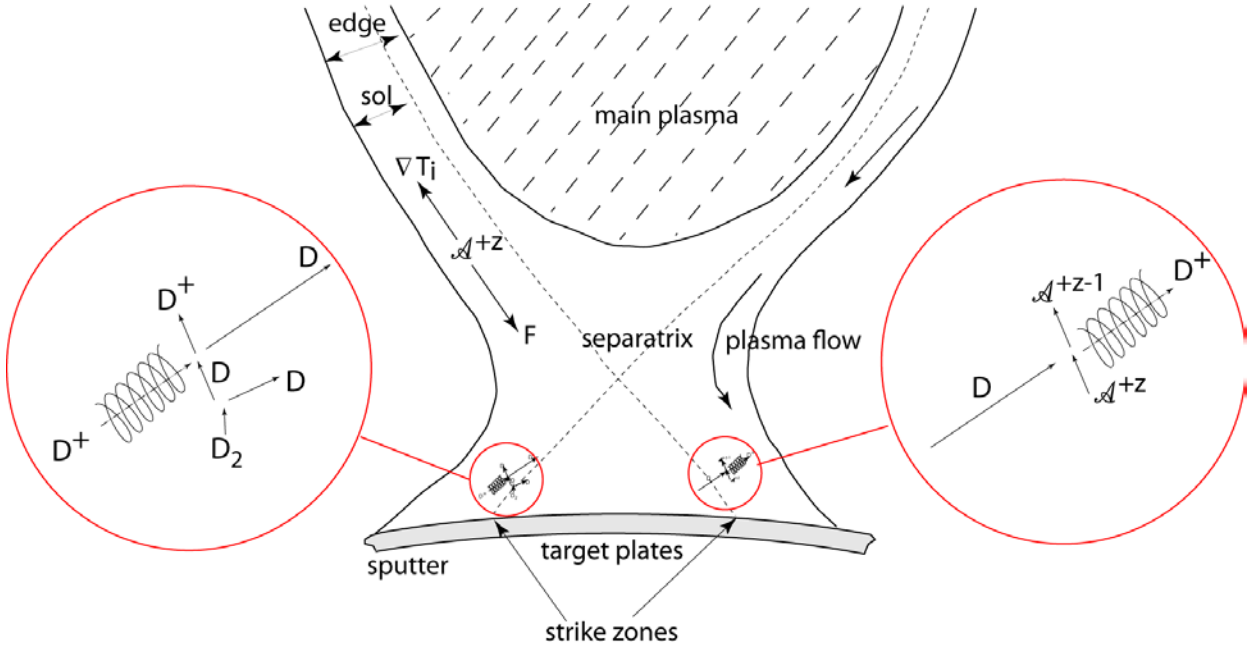

The migration of D^0 into the plasma is more efficient than expected since the CX reaction rate is larger than the electron impact ionisation rate for D^0 .

$$D(1s) + D^+ \rightarrow D^+ + D(1s)$$

$$D(1s) + e \rightarrow D^+ + e + e$$

The partially ionised impurities near the wall have shells of existence which can overlap that of D^0. The charge transfer at thermal speeds is very strongly state- selective with only one or two states significantly populated. The reaction is in competition with electron impact excitation from the ground or metastable levels.

$$\mathcal{A}^{+z}(\nu) + D(1s) \rightarrow \mathcal{A}^{+(z-1)}(i) + D^+$$

$$\mathcal{A}^{+z}(\nu) + D(n=2) \rightarrow \mathcal{A}^{+(z-1)}(i) + D^+$$

$$\mathcal{A}^{+(z-1)}(\rho) + e \rightarrow \mathcal{A}^{+(z-1)}(i) + e$$

Ratios of spectrum lines emitted by $\mathcal{A}^{+z-1}$ can be altered modestly. The bigger effect is the change of ionisation state. The ADAS codes ADAS208 and ADAS405, including H-lines in the adf04 dataset model this emission.

1.2 CX reaction rates and impurity spectral emission in divertors

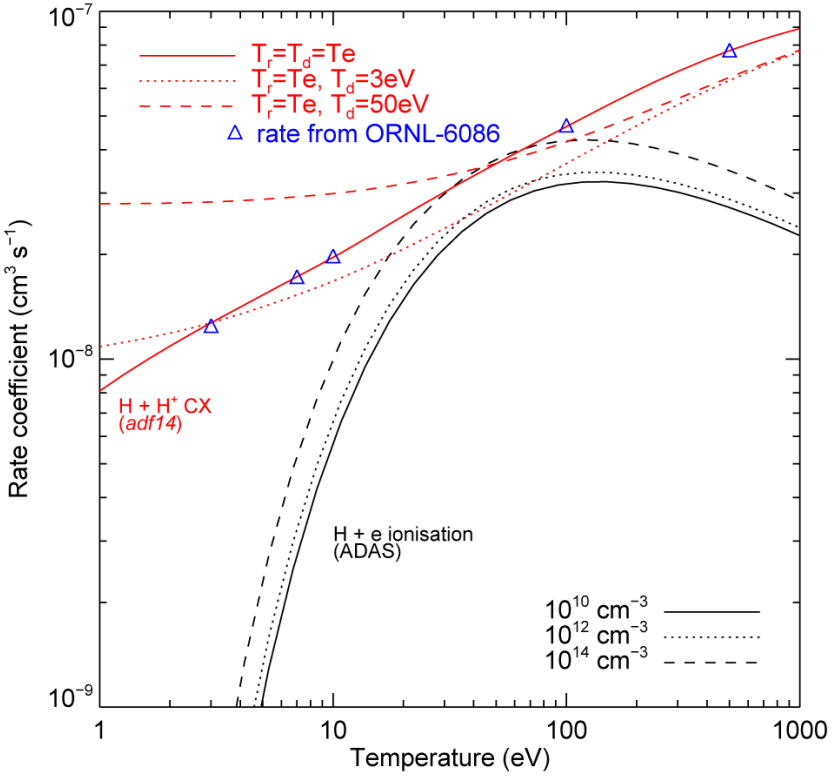

Comparative reaction data electron impact and ion impact are available in ADAS. With ion/atom rates, the distribution functions of both reactants matter.

ADAS data formats *adf14* and adf24 are relevant to charge exchange in thermal conditions. ADAS509 and the procedure *ceevth.pro* are helpful.

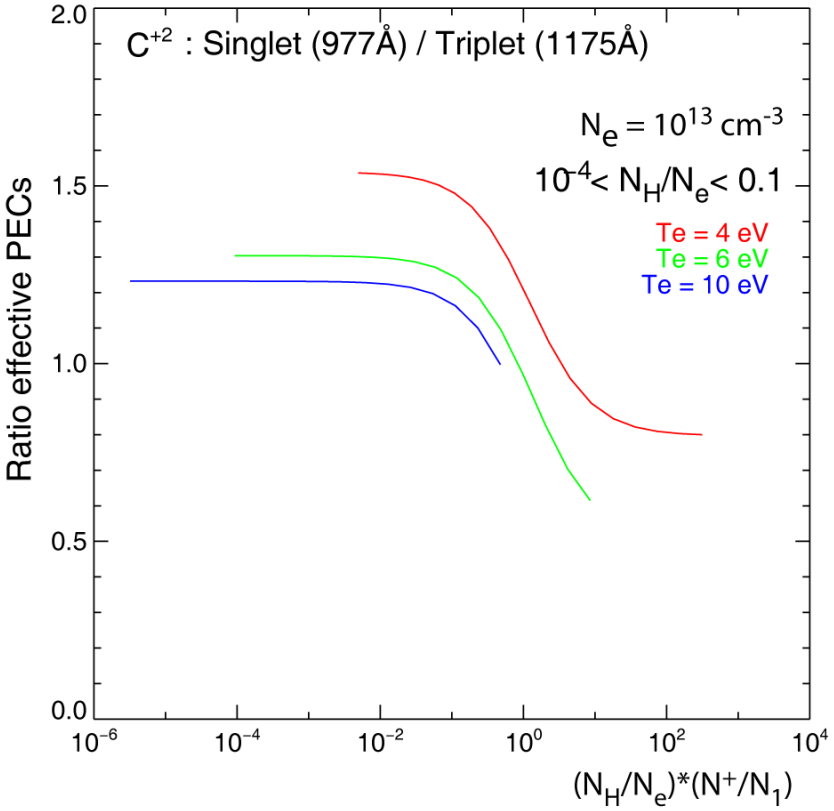

Thermal charge transfer from hydrogen to impurity ions is a very state-selective process. It competes with the generally stronger electron impact excitation. Depending on divertor conditions, emission measures may be favourable for diagnostic line ratios. *adf15* includes CX contributions.

1.3 The beam plasma environment

The injected neutral atoms, usually isotopes of hydrogen, have speeds comparable to the Bohr orbital speed (≡ 25keV/amu).

Positive ion sources have acceleration voltages ~40-160keV. For hydrogen isotopes, the neutral beam contains three energy fractions, E_b, $E_b/2$ and $E_b/3$ of varying proportions. These energies are well suited to CXRS.

^{2}D is the most commonly injected hydrogen isotope. Also ^{3}He and ^{4}He have been used, usually as minority admixtures to hydrogen. All can be handled with ADAS.

Negative ion sources (hydrogen isotopes) usually operate at acceleration voltages >200keV and give mono-energetic neutral beams. These energies are less suited to CXRS.

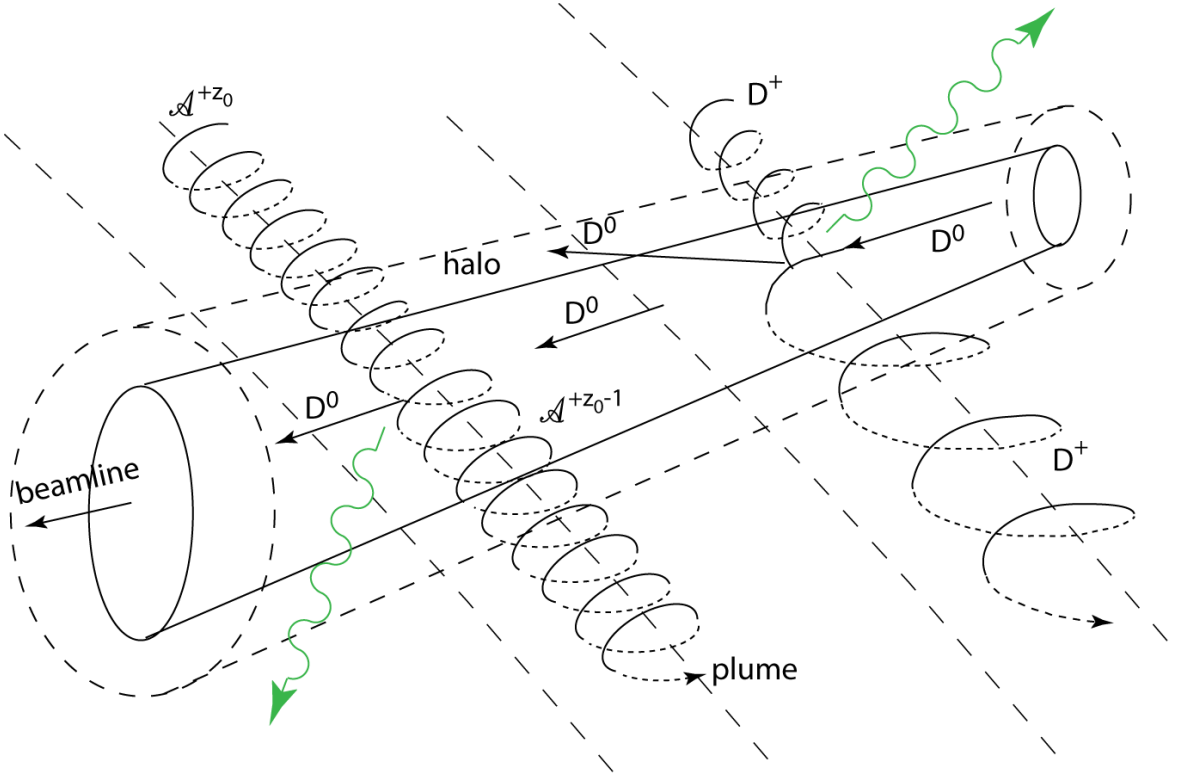

In the core plasma, with T_i ~6keV, a carbon nucleus has average energy 0.5keV/amu << E_b so the beam speed usually determines the collision speed of projectile (D^0 donor) and target($\mathcal{A}^{+Z_0}$ receiver). This situation is reversed for electron collisions with both donors and receivers.

$\mathcal{A}^{+Z_0-1}$ is the CX emitter. The halo radius is an ionisation length. The key plume length is a radiative decay length.

1.4 Reactions in the beam plasma region

- Charge exchange spectroscopy is driven by reactions of the form.

$$X^{+z_0} + D^0_{beam}(1) \rightarrow X^{+z_0}(nl) + D^+_{beam}$$

- The principal application is to capture by the bare nuclei of impurity atoms in the plasma from the ground state of deuterium in fast neutral beams. The hydrogen-like impurity ion radiates as

$$X^{+z_0-1}(n'l') \rightarrow X^{+z_0-1}(n''l'') + h\nu$$

- Composite spectral line features of the form $n' \rightarrow n''$ are observed made up of unresolved multiplet components. Charge exchange line features often involve high principal quantum shells and occur over wide spectral ranges including the visible.
- In general the populations of receiver levels are modified by redistributive collisions with plasma ions, electrons and fields before radiation emission occurs.

1.5 Partial capture cross-section behaviours.

Partial n and partial nl CX cross-sections

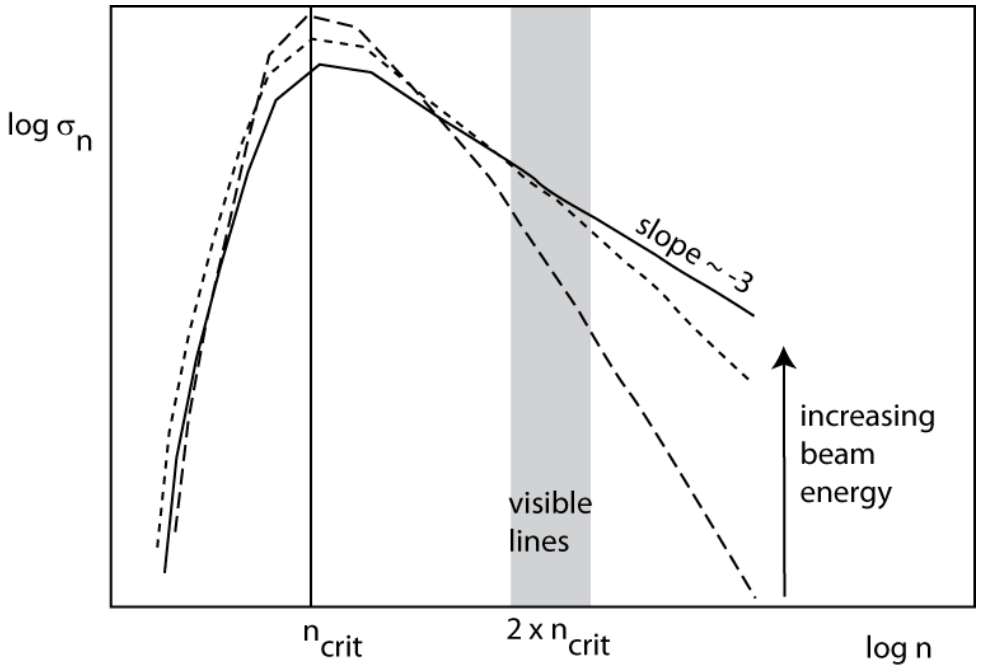

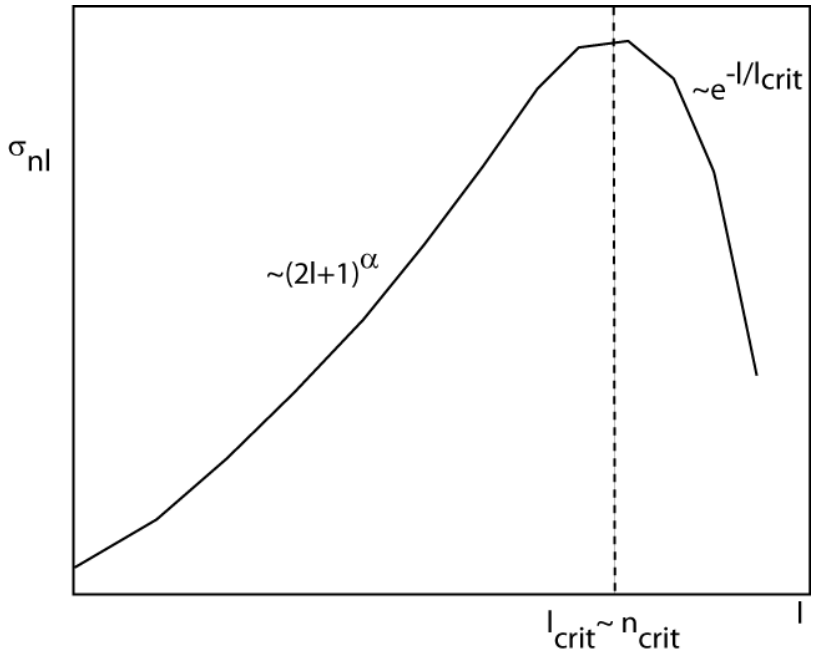

- Asymptotic slope in n at higher beam energies means that cascading contributions to populating of emitting levels are significant.

1.6 adf01 format and extrapolation parameters

n-shells above the numerical tabulation contribute substantially to effective emission in visible CX lines.

Asymptotically

$$\sigma_n(E_u) = \left(\frac{n_t}{n}\right)^{\alpha(E_u)} \sigma_{n_t}(E_u)$$

for $n > n_t$

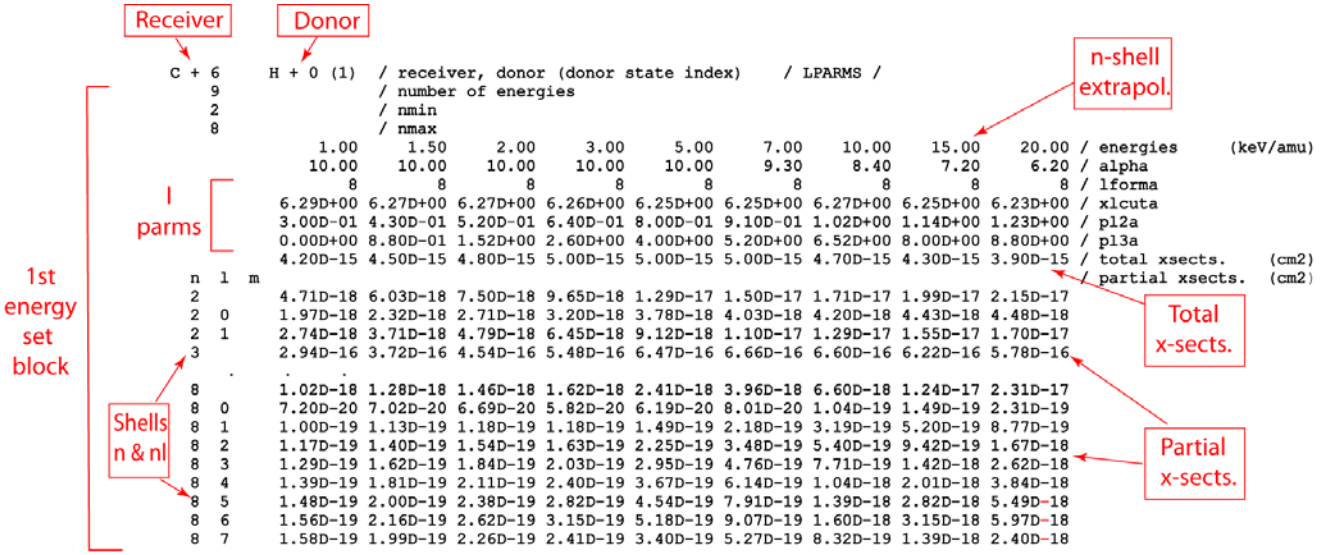

To a reasonable approximation, there is universal scalable behaviour in l so that for the capture cross-sections.

$$\sigma_{nl}(E_u) = f^{(theor)}_{(n)l}\, \sigma_n(E_u)$$

$$f^{(theor)}_{(n)l} = \left(\frac{1}{2}\right)[1 - \tanh(w(l - l_{cut}))]\left(\frac{2l+1}{2l_{cut}+1}\right)^{p_2} + \left(\frac{1}{2}\right)[1 + \tanh(w(l - l_{cut}))]\exp(p_3(1 - l/l_{cut}))$$

Of various forms investigated the preferred one for ADAS is shown on the right (lforma = 8).

with $w = 1.2$, $p_2 \equiv$ pl2a, $p_3 \equiv$ pl3a, $l_{cut} \equiv$ xlcuta

2.1 Population structure: bundle-nl with CX

CX enhancement

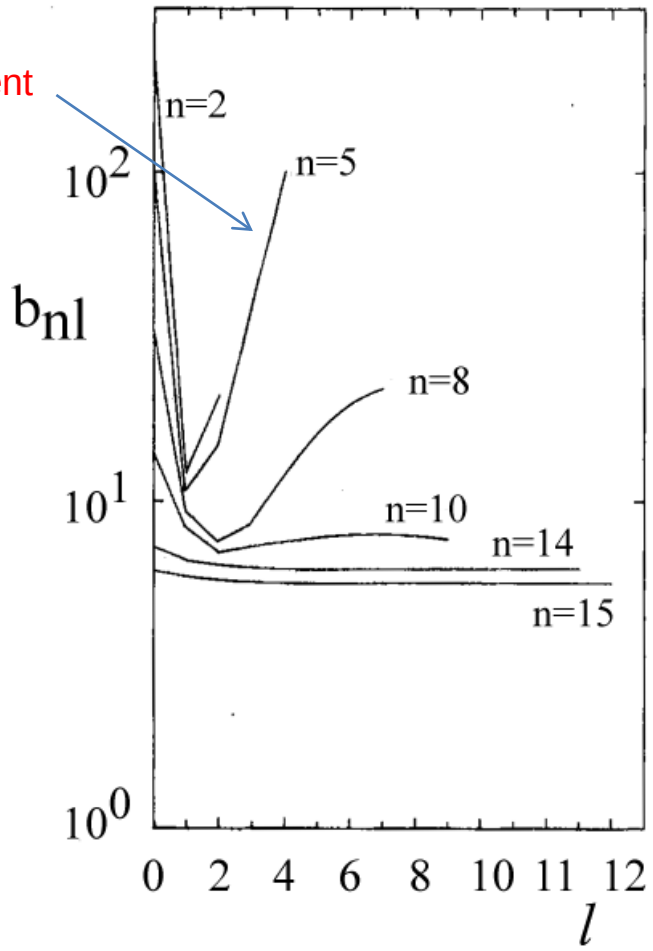

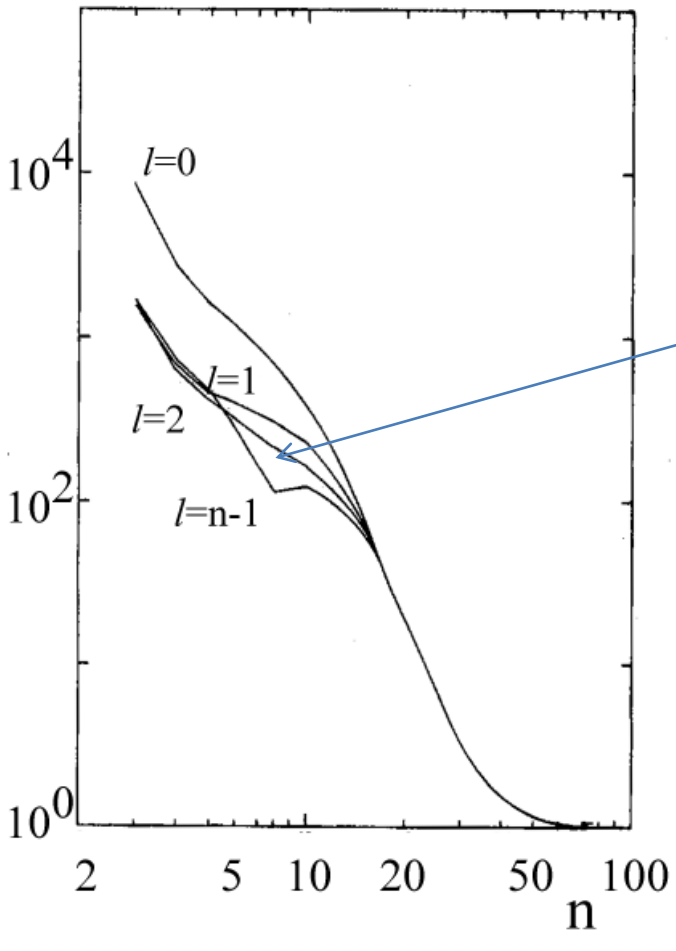

roll-off above n_{crit}

O^{+7} : $T_e=T_p=6.4x10^6$, $N_e=N_p=5x10^{13}$ cm^{-3}, $E_H=25keV/amu$, $N_H=5x10^7$ cm^{-3}

O^{+5} : $T_e=T_p=3.6x10^6$, $N_e=N_p=5x10^{13}$ cm^{-3}, $E_H=25keV/amu$, $N_H=5x10^8$ cm^{-3}

2.2 The redistribution-cascade population model

- With the dominant collisional-radiative processes state selective capture, collisional redistribution by ions within each n-shell and cascade, the effective emission coefficient determination simplifies. It can be implemented recursively downwards. Relevant matrices may be stored to enable a multi-line experimental confrontation.

Since no collisional excitation from lower to higher n-shells is allowed, the populations of the lj sub-levels of the principal quantum shell $n' \geq n+1$ may be written as

$$N_{n'l'j'} = N_H N^+ \sum_{n''\geq n+1} W_{n'l'j',n^{iv}} q^{(CX)}_{n^{iv}}$$

Then the equations determining the populations of the sub-shells of the principal quantum shell n are

$$\sum_{l''j''} M_{(n)lj,l''j''} N_{nl''j''} = N_H N^+ f^{(theor)}_{(n)lj} q^{(CX)}_n + \sum_{n'\geq n+1} A_{nlj,n'l'j'} N_{n'l'j'}$$

so that

$$N_{nlj} = N_H N^+ W_{nlj,n} q^{(CX)}_n + N_H N^+ \sum_{n^{iv}\geq n+1} W_{nlj,n^{iv}} q^{(CX)}_{n^{iv}}$$

with

$$W_{nlj,n} = [\sum_{l'',j''} M^{-1}_{(n)lj,l''j''} f^{(theor)}_{(n)l''j''}] q^{(CX)}_n$$

and

$$W_{nlj,n^{iv}} = \sum_{l'',j'',l',j'} M^{-1}_{(n)lj,l''j''} A_{nl''j'',n'l'j'} W_{n'l'j',n^{iv}}$$

2.3 *adf12* charge exchange effective emission coefficients

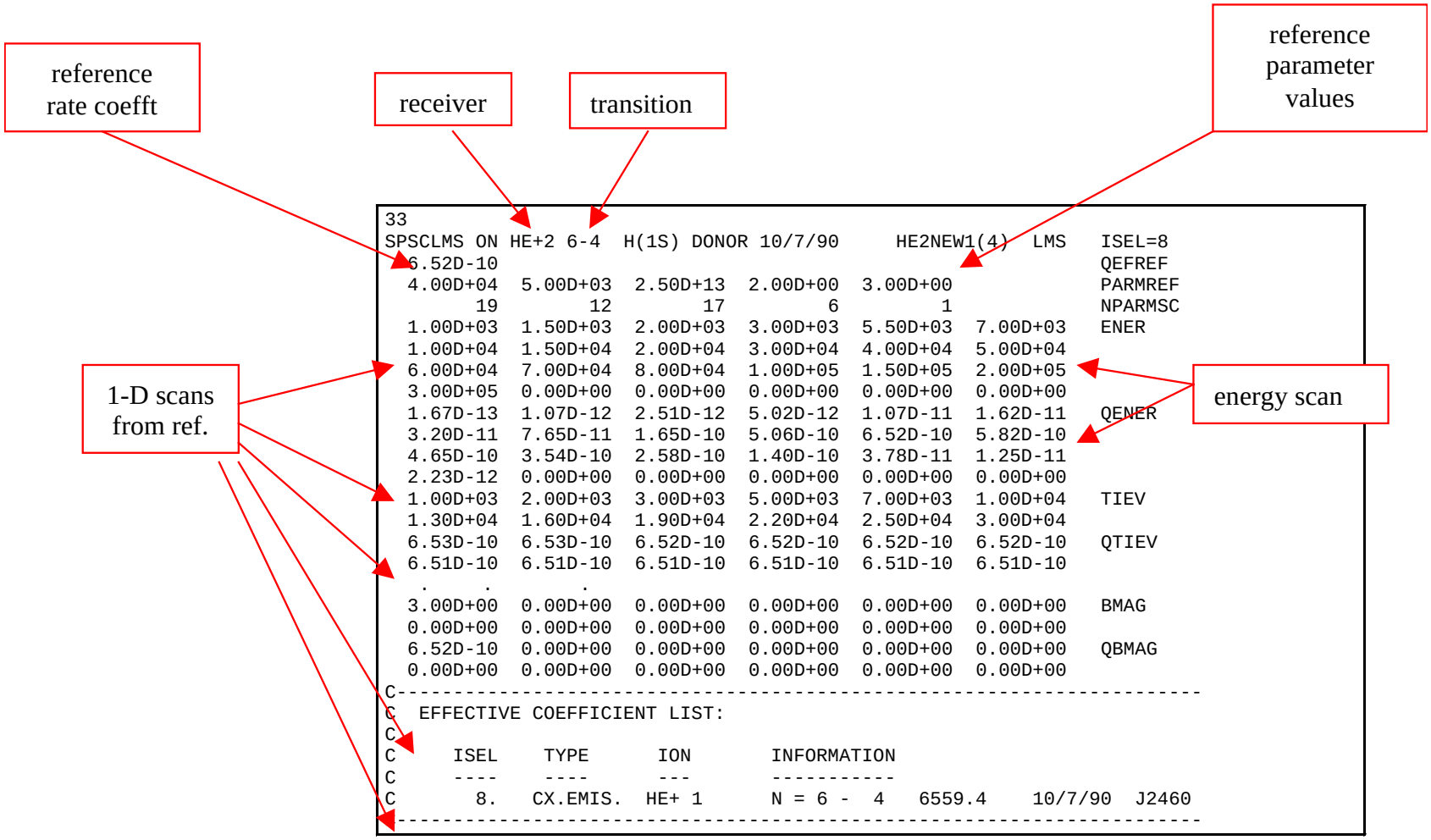

3.1 Line-of-sight emission

- The line-of-sight integrated photon emissivity of a charge exchange driven line may be written as

$$
\begin{aligned}
I_{n\to n'}^{(z_0-1)} &= \sum_{l,l'} I_{nl\to n'l'}^{(z_0-1)} \\
&= \int_S \sum_{l,l'} A_{nl\to n'l'} N_{nl}^{(z_0-1)} ds \\
&= \int_S [\sum_{l,l'} A_{nl\to n'l'} (N_{nl}^{(z_0-1)} \ / \ N_D N^{(z_0)})] N_D N^{(z_0)} ds \\
&= \int_S [\sum_{l,l'} q_{nl\to n'l'}^{(eff)}] N_D N^{(z_0)} ds \\
&= \int_S q_{n\to n'}^{(eff)} N_D N^{(z_0)} ds \\
&\approx q_{n\to n'}^{(eff)} \int_S N_D N^{(z_0)} ds
\end{aligned}
$$

- $\int_S N_D N^{(z_0)} ds$ is the emission measure
- $q_{n\to n'}^{(eff)}$ is the effective emission coefficient

3.2 Charge exchange emission measure

- The effective emission coefficient may be obtained theoretically from a collisional-radiative population calculation.
- If it is approximately constant over the emitting volume, then measurement of a charge exchange line intensity $I_{n\to n'}^{(z_0-1)}$ allows deduction of the emission measure

  .

$$\int_S N_D N^{(z_0)} ds$$

- If neutral beam attenuation to the observed volume is known or calculable then the local impurity number density may be inferred.
- With the effective emission coefficients calculated theoretically, comparison with one charge exchange line intensity allows deduction of the emission measure. Then all other lines are predictable.
- If more than one line intensity is observed then a mean emission measure may be deduced and some comment made on the ratios of experimental to theoretical effective emission coefficients.

3.3 Effective emission coefficients for various beam donors

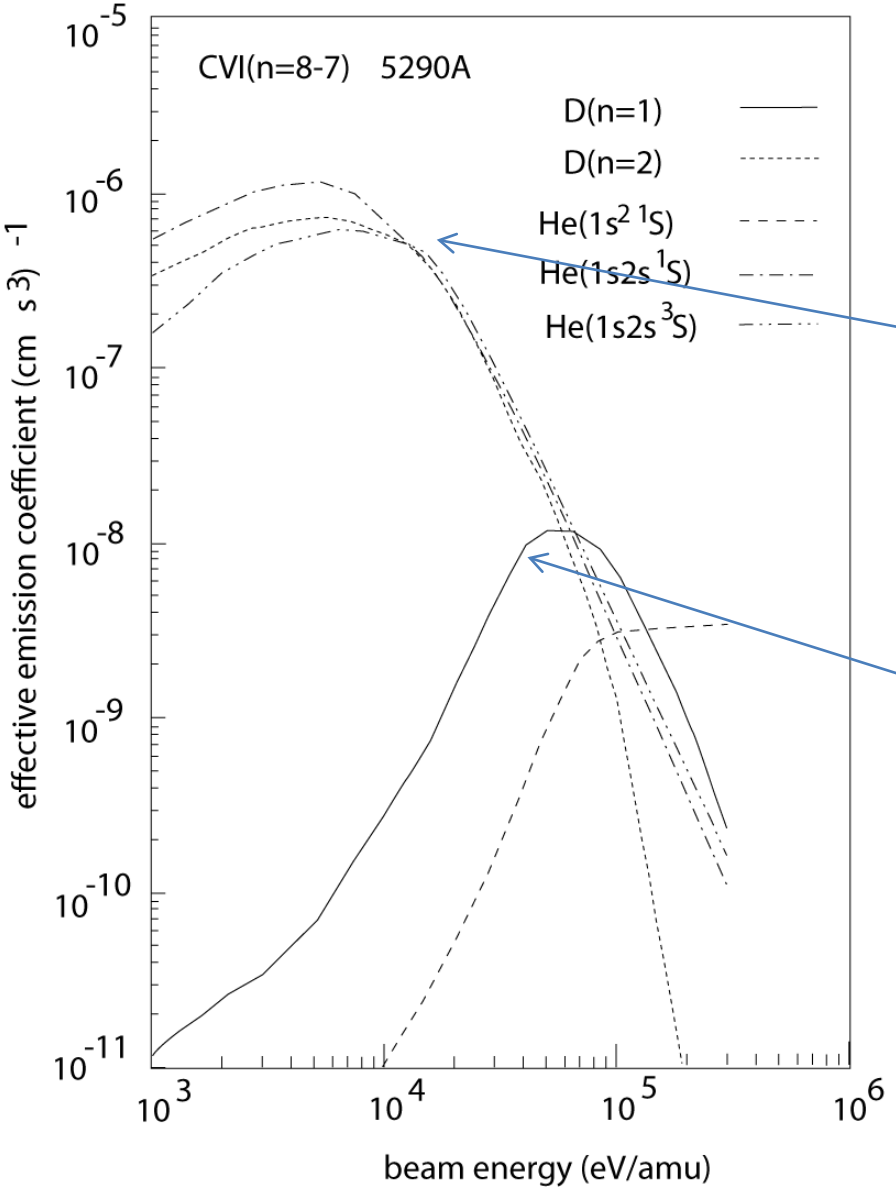

excited donor effective emission coefficients are much larger at lower beam energies

The ratio of the excited donor population to that of the ground state donor means that ground state door effective emission is greater above ~20keV/amu

3.4 Consistency of observed spectral intensities

In general observable spectrum lines are associated with upper principal quantum shells $n \le n_1$. If M_{rep}, lines are identified each with a distinct upper n-shells $\overline{n}_{irep} : irep = 1, \ldots, M_{rep}$, then a 'condensation' may be imposed such that

$$q_n^{(CX)} = \sum_{irep=1}^{M_{rep}} L_{n,irep} q_{\overline{n}_{irep}}^{(CX)} \qquad \text{for } n_0 \le n \le n_1$$

and

$$q_n^{(CX)} = (n / n_1)^{\alpha} q_{n_1}^{(CX)} \qquad \text{for } n > n_1$$

giving, after integration along the line-of-sight, a matrix relation

$$\begin{bmatrix} I_{\overline{n}_1 \to \overline{n}_1'} \\ . \\ I_{\overline{n}_{M_{rep}} \to \overline{n}_{M_{rep}}'} \end{bmatrix} = \left(\int_S N_D N^+ ds\right) \begin{bmatrix} a_{11} & . & . & a_{1 M_{rep}} \\ . & . & . & . \\ a_{M_{rep} 1} & . & . & a_{M_{rep} M_{rep}} \end{bmatrix} \begin{bmatrix} q_{\overline{n}_1}^{(CX)} \\ . \\ q_{\overline{n}_{M_{rep}}}^{(CX)} \end{bmatrix}$$

The coefficients of the matrix are theoretically calculated quantities. The equations may be solved for the the $q_{\overline{n}_i}^{(CX)}$ and the emission measure $\int_S N_D N^+ ds$ subject to the constraint

$$\sum_{irep=1}^{M_{rep}} q_{\overline{n}_{irep}}^{(CX)} = \sum_{irep=1}^{M_{rep}} q_{\overline{n}_{irep}}^{(CX)(theor)}$$

- This casts the theory/experiment challenge in terms of the partial n-shell charge exchange cross-sections – an important issue as CXS with heavier species is contemplated.

4.1 Beam stopping and emission

To progress further with charge exchange spectral analysis, that is to unfold the emission measure, it is necessary to know the local number density of beam atoms in the plasma at each point along the beam. The hydrogen isotopes species H, D and T and the helium isotopes ^{3}He and ^{4}He must be addressed for comprehensive coverage of fusion needs.

The isotope mass influences the beam speed. The fundamental collision cross-sections, as a function of relative collision speed are the same. So rate coefficients, for atom-ion collisions must use the correct speeds. Otherwise beam population and collisional-radiative modelling are the same.

Hydrogen isotope beams: collisionality is strong, the collision limit is typically ~n=4, l-sub-shells are strongly mixed. Bundle-n modelling is appropriate for the beam populations. The stopping coefficient is the $S_{CR,\,1s\,^2S}$ coefficient (including charge exchange losses) of the ground level. Excited beam populations are solved as

$$b_n = F_n^{(1)}\frac{N_1}{N_+} + F_n^{(2)} + F_n^{(3)}\frac{N_H}{N_e}$$

Helium isotope beams: collisionality is strong, the collision limit is typically n ~ 4, l-sub-shells are less strongly mixed. There are two effective metastables, the ground $1s^2\ ^1S$ and the triplet $1s2s\ ^3S$ (often $1s2s\ ^1S$ is also treated as metastable for consistency with other applications). The singlet and triplet sides behave like two almost independent beams with stopping coefficients $S_{CR,\,1s^2\,^1S}$ and $S_{CR,\,1s2s\,^3S}$. Bundle-nl modelling is appropriate. Excited populations are solved as

$$b_{nl^{2S+1}L} = FI^{(1)}_{(nlS)}\left(\frac{N_{1^1S}}{N_+}\right) + FII^{(1)}_{(nlS)}\left(\frac{N_{2^1S}}{N_+}\right) + FIII^{(1)}_{(nlS)}\left(\frac{N_{2^3S}}{N_+}\right) + F^{(2)}_{(nlS)} + F^{(3)}\left(\frac{N_H}{N_e}\right)$$

4.2 Beam atom population modelling and stopping

For beam atom populations, collisions with impurity ions must be added to the rate equations and the beam translational speed added to collision dynamics to form the rate coefficients. In ADAS, adf02 provides the ion impact cross-section data. adf07 provides the most accurate electron impact direct ionisation coefficients.

The ADAS data format adf21 and adf22 archive the beam stopping and beam emission coefficients. They are held in libraries for the different beam species in datasets for each individual impurity species which contributes to the stopping (see next viewgraph).

The beam energy and impurity number density are the primary parameters, with other secondary. This determines the organisation of the adf21 and adf22 archives.

Beam stopping by a composite of impurities and electrons is usually assembled as a linear superposition of pure stopping species.

The beam stopping coefficient is defined in terms of the electron density.

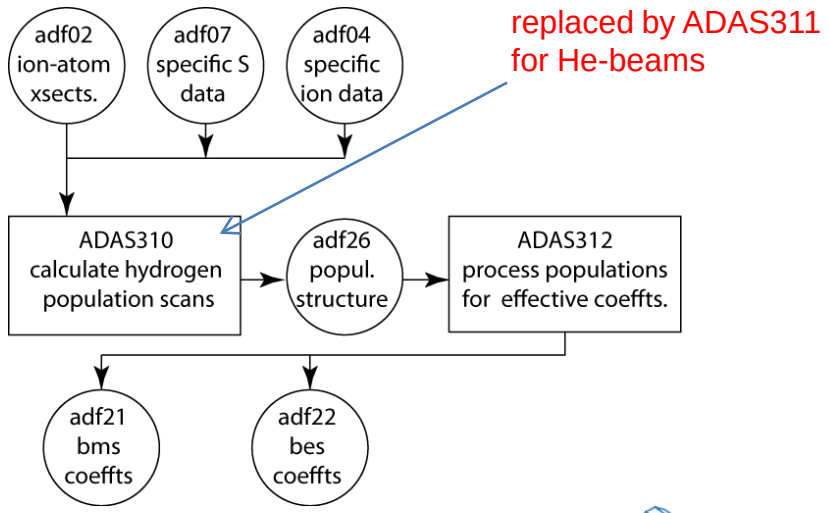

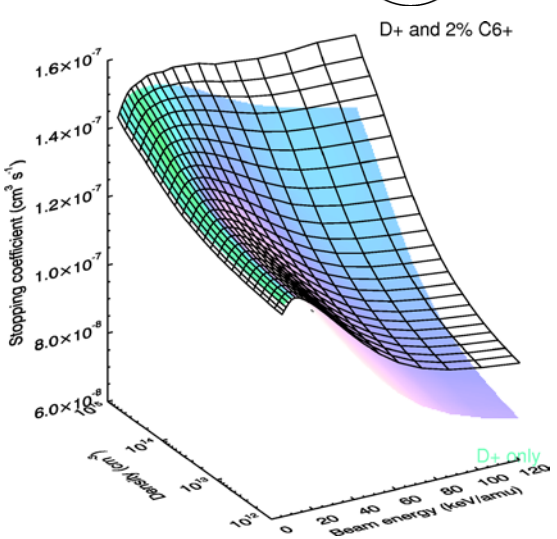

Stopping coefficient for D-beam in $2x10^3$ eV D^+ +2% C^{+6} plasma.

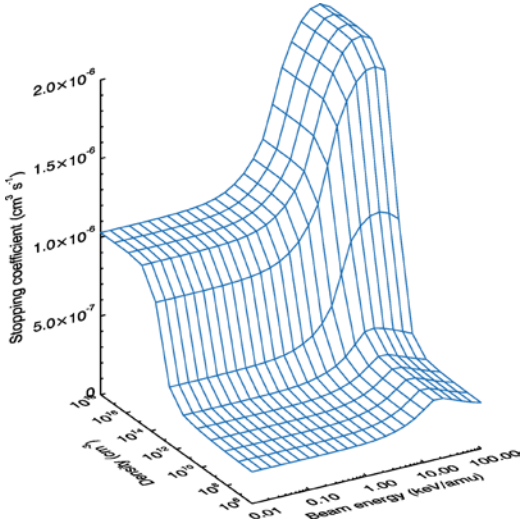

Stopping coefficient for the He-beam triplet metastable by a pure D+ plasma at $2x10^3$ eV.

4.3 Assembling beam stopping coefficients

Let the stopping coefficient for the impurity species X^{+z_0} be $S_{CR}^{(\mathcal{A},X)}$ then the loss rate is

$$N_e S_{CR}^{(\mathcal{A},X)}(E_B, N^{(z_0)}, T^{(z_0)}) = N_e S_{CR}^{(\mathcal{A},e)}(E_B, N^{(z_0)}, T^{(z_0)}) + N^{(z_0)} S_{CR}^{(\mathcal{A},z_0)}(E_B, N^{(z_0)}, T^{(z_0)})$$

distinguishing parts driven by excitation from the ground state of A by electron collisions and by X^{+z_0} ions respectively. The coefficient is

$$S_{CR}^{(\mathcal{A},X)}(E_B, N^{(z_0)}, T^{(z_0)}) = S_{CR}^{(\mathcal{A},e)}(E_B, N^{(z_0)}, T^{(z_0)}) + (1/z_0) S_{CR}^{(\mathcal{A},z_0)}(E_B, N^{(z_0)}, T^{(z_0)})$$

The density dependence of the collisional-radiative coefficient is written in terms of the impurity ion density $N^{(z_0)}$ since ion collisions primarily determine the collisional redistribution..

Consider a set of species $\{X_i^{+z_{0i}} : i = 1,..,I\}$ with fractions $\{f_i : i = 1,..,I\}$, in the plasma causing a composite stopping. The loss rate may be written approximately as

$$N_e S_{CR}^{(\mathcal{A})}(E_B, N_I, T_I) \approx N_e S_{CR}^{(\mathcal{A},e)}(E_B, N_I, T_I) + \sum_{i=1}^{I} N_i^{(z_{0i})} S_{CR}^{(\mathcal{A},z_{0i})}(E_B, N_I, T_I)$$

$$= \sum_{i=1}^{I} N_{e,i} [S_{CR}^{(\mathrm{A},e)}(E_B, N_I, T_I) + (1/z_{0i}) S_{CR}^{(\mathrm{A},z_{0i})}(E_B, N_I, T_I)]$$

ADAS304 interrogates the data formats adf21 and adf22 and assembles mixtures.

where

$$N_e = \sum_{i=1}^{I} N_{e,i} = \sum_{i=1}^{I} z_{0i} N^{(z_{0i})} = N_I (\sum_{i=1}^{I} z_{0i} f_i)$$

defines the proportions of the electron density contributed by each impurity species.

4.4 D(n=3-2) beam emission

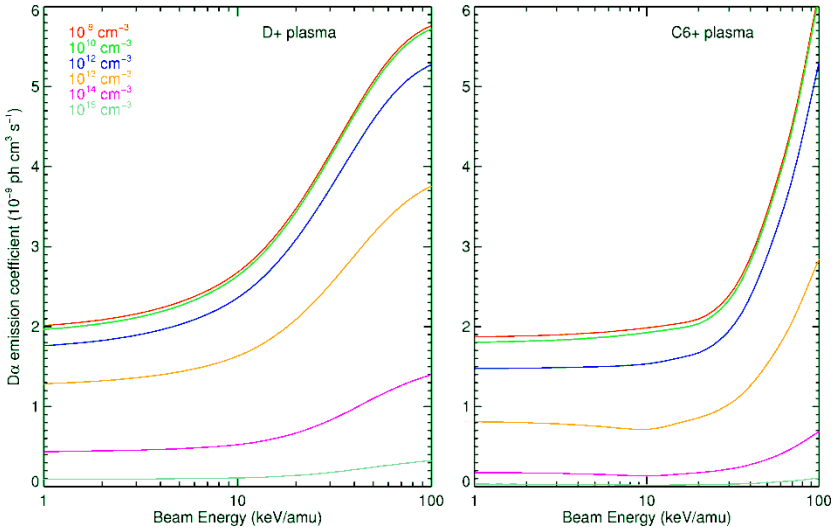

The beam emission lines appear Doppler shifted as Stark multiplets due to the motional electric field in the beam atom frame.

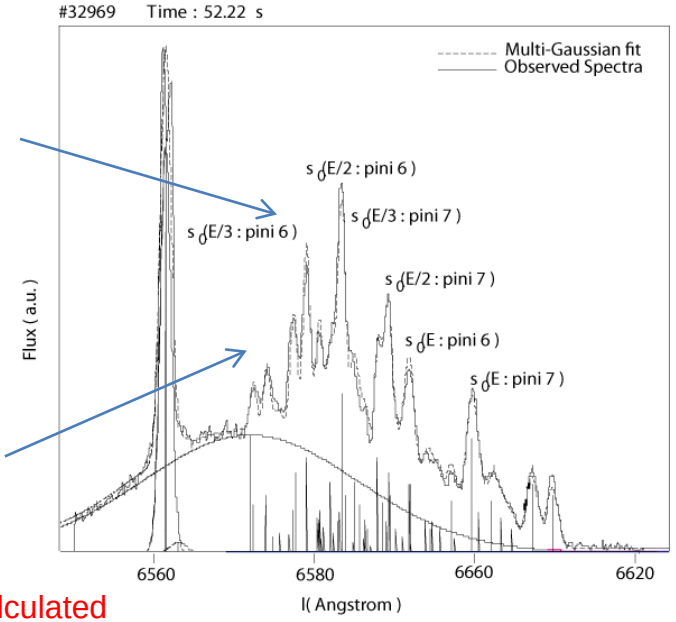

Observed beam emission spectrum.

The bundle-n model works well for overall H-beam Balmer line intensities and ratios. Although l-mixing is substantially complete at most densities, the subtlety of the motional Stark features justifies more elaborate studies, linked to MSE spectroscopy.

D(n=3-2) calculated pattern for one beam fraction.

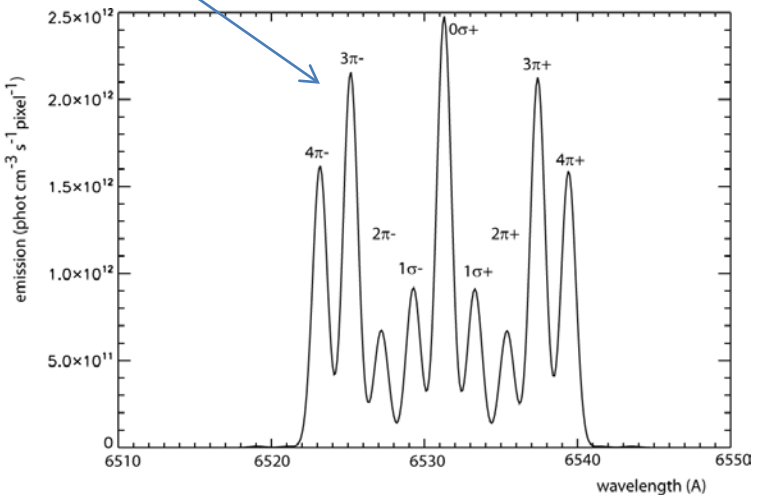

Stark resolved collisional radiative models seek to describe the precise wavelengths, the polar distribution and polarisation of emission and the collisional mixing for the low n-shell emission (Balmer and Paschen). See for example adas305_get_stark.pro.

4.5 Calculating Stark manifold populations and emission

The Hamiltonian for the beam hydrogen atom crossing the magnetic field strength $\vec{\mathcal{B}}$ with velocity $\vec{v}_b$ is

$$H = H_0 - e\vec{\mathcal{E}}_m \cdot \vec{r} - e\vec{\mathcal{E}} \cdot \vec{r} - \vec{\mu} \cdot \vec{\mathcal{B}}$$

where $\vec{\mathcal{E}}_m = \vec{v}_b \wedge \vec{\mathcal{B}}$ is the motional Stark electric field.
$\vec{\mu} = \mu_0(\vec{L} + 2\vec{S})$ is the magnetic moment of the electron in the atom.
H_0 is the isolated atom Hamiltonian.

Diagonalise this Hamiltonian in a basis of zeroeth order wave functions of the isolated atom. In ADAS, this is done for each n-shell separately. With only the $\vec{\mathcal{E}}_m$ field, we obtain Stark states as labelled below, where the axis of quantisation is along $\vec{\mathcal{E}}_m$.

n=3 energy levels of hydrogen in Stark field

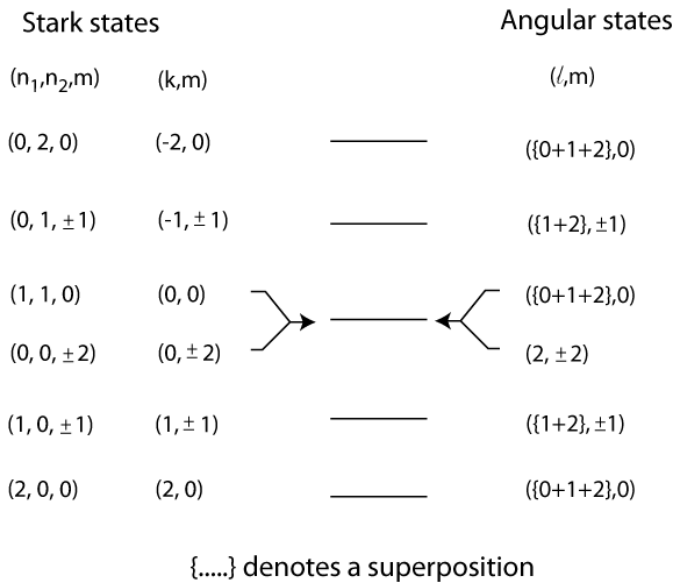

{.....} denotes a superposition

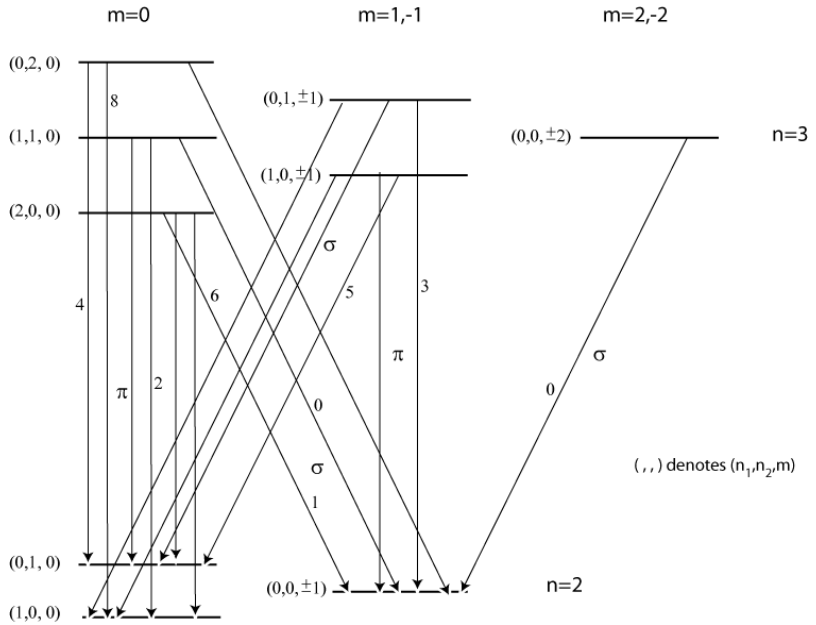

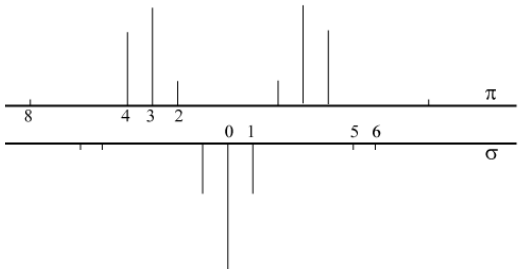

For the pure Stark field case the n=3-2 transitions are as above giving the spectrum shown on the previous viewgraph. The code adas305_get_stark.pro does this for arbitrary fields and orientations.

5.1 Integrated analysis

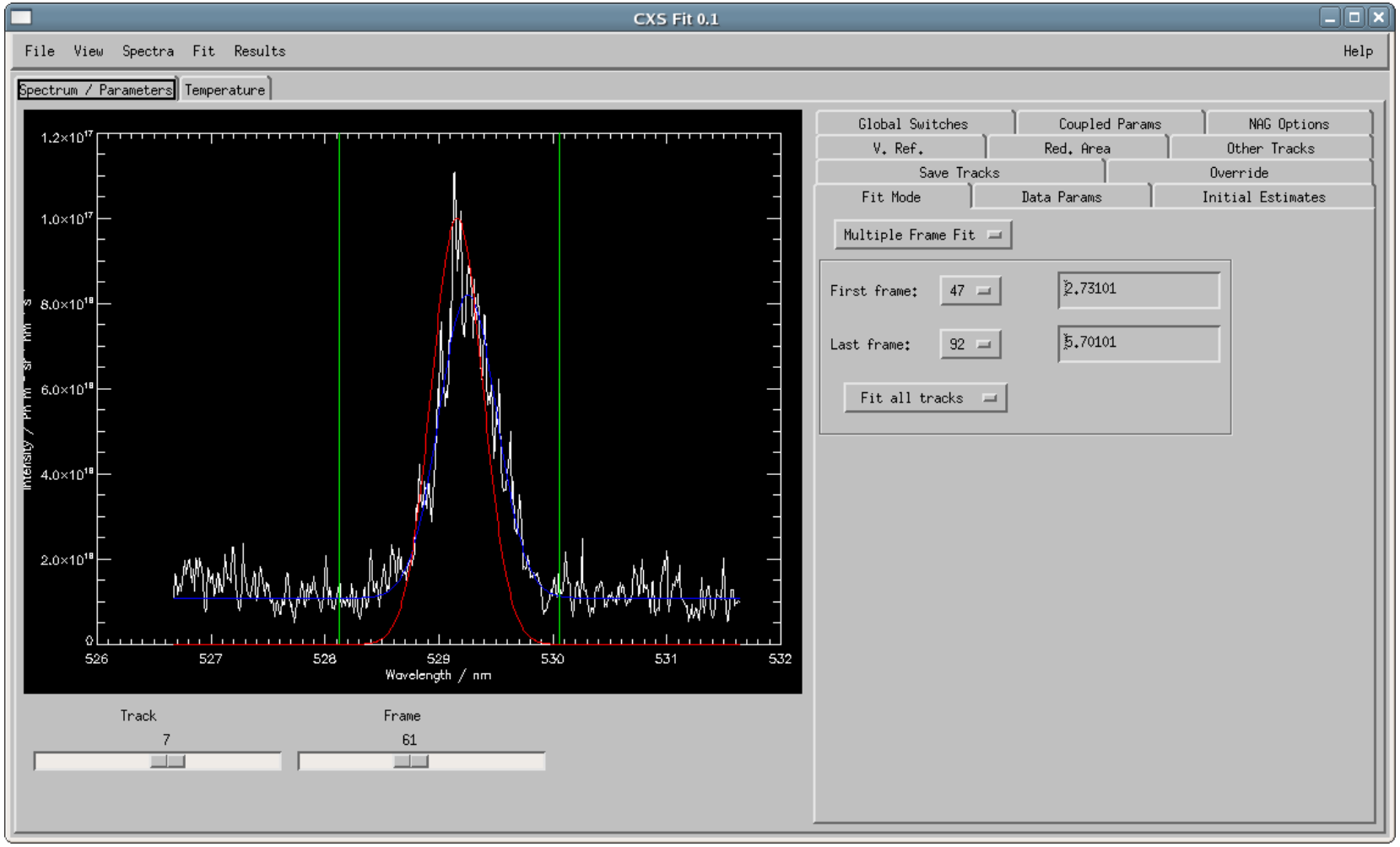

The codes CXSFIT, UTC and CHEAP, maintained by the ADAS team, assist in diagnostic analysis using charge exchange driven spectral features.

6.1 Conclusions

- Charge exchange is a key atomic reaction in fusion plasmas with special diagnostic impact when the donor atom, usually hydrogen or helium isotopes, is in a fast beam.

- Charge exchange in the thermal edge-divertor plasma is a strongly state selective process which can modify line ratios and ionisation balance of light impurities.

- Charge transfer from fast beam atoms can populate subdominant levels of the receiver ions in the plasma giving visible emission and enabling charge exchange spectroscopy (CXS).

- Collisional-radiative modelling is required to predict CXS emission. Special models and analysis tools allow diagnostic insight and extraction of plasma parameters. ADAS has extensive data collections and models to support such analysis and for preparation of new derived data.

- Beam stopping and beam emission are key consequences of the interaction of the beam atoms with the plasma. The beam emission is of special diagnostic importance, enabling beam emission spectroscopy (BES).

- Collisional-radiative models for beam atoms are strongly affected by ion collisions. ADAS has extensive data collections and models to support these situations and analyses.

- The influence of the motional Stark electric field on beam atoms crossing the containment magnetic field of the plasma is an exotic effect and powerfully diagnostic. Special ADAS models allow exploration of this and related effects – see also module 6.